

PAPER • OPEN ACCESS

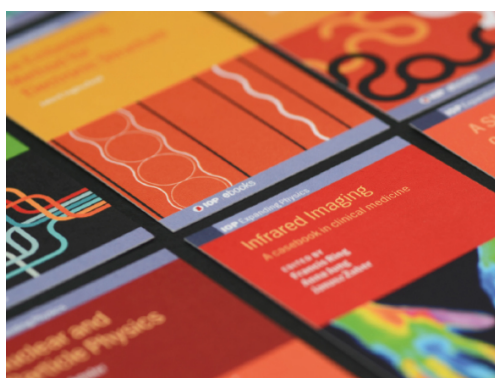
White-light versus discrete wavelength measurements of Faraday dispersion and the Verdet constant

To cite this article: James L Maxwell *et al* 2022 *Eur. J. Phys.* **43** 015302

View the [article online](#) for updates and enhancements.

You may also like

- [Thermooptics of magnetoactive media: Faraday isolators for high average power lasers](#)
E A Khazanov
- [Verdet constant determination of dielectric media using a new versatile, portable and low-cost magneto-optical rotator](#)
Watheq Al-Basheer
- [A modulation technique for the measurement of the DC longitudinal Faraday effect](#)
Carlos Hunte



IOP | ebooks™

Bringing together innovative digital publishing with leading authors from the global scientific community.

Start exploring the collection—download the first chapter of every title for free.

White-light versus discrete wavelength measurements of Faraday dispersion and the Verdet constant

James L Maxwell , Ifan G Hughes*  and Charles S Adams*

Physics Department, Durham University, Durham DH1 3LE, United Kingdom

E-mail: i.g.hughes@durham.ac.uk and c.s.adams@durham.ac.uk

Received 28 July 2021, revised 28 September 2021

Accepted for publication 20 October 2021

Published 11 November 2021



Abstract

The wavelength dependence of the Faraday effect may be measured either sequentially at particular wavelengths using narrow band sources, or simultaneously at many wavelengths using a white-light or broadband source. We apply both methods to measure the wavelength dependence of the Verdet constant of a terbium gallium garnet crystal. We show that although the white-light measurement offers the advantage of requiring only one source, it is more prone to systematic errors than using multiple laser sources.

Keywords: TGG, Faraday dispersion, spectroscopy

(Some figures may appear in colour only in the online journal)

1. Introduction

In 1845 Michael Faraday made a key step in the unification of optics and electromagnetism with the discovery that a magnetic field changes the polarization of light propagating in a medium [1]. In the modern era, the Faraday effect is particularly important in laser physics where it is used to realise an optical diode—a device that transmits light in only one direction [2–4], and in Faraday filtering, where Faraday dispersion allows the realisation of narrowband filters [5–14], which are important for atmospheric and solar monitoring [15–20]. For most applications, an optical medium with a combination of high optical transmission and large Faraday effect is desirable [4, 21–25].

*Authors to whom any correspondence should be addressed.



Original content from this work may be used under the terms of the [Creative Commons Attribution 4.0 licence](https://creativecommons.org/licenses/by/4.0/). Any further distribution of this work must maintain attribution to the author(s) and the title of the work, journal citation and DOI.

The Faraday rotation of the plane of polarization of light with wavelength λ in a medium with length l is given by

$$\theta_B(\lambda) = V(\lambda)Bl, \quad (1)$$

where $V(\lambda)$ is the Verdet constant, and B is the average magnetic field strength along the medium. Note that the magnetically induced rotation $\theta_B(\lambda)$ is a function of the wavelength λ , i.e. the Verdet constant depends on λ . This effect is known as Faraday dispersion and can be understood by considering linearly polarised light to be an equal superposition of right and left circular polarisations. In the presence of a magnetic field, a Faraday medium will become birefringent; exhibiting different right and left circular refractive indices. The two circular polarisations of the input field will thus propagate relative to one another in the medium and will incur a relative phase shift [1]. This is equivalent to a rotation in the linear polarisation. At room temperatures, the primary contribution to the birefringence is caused by a splitting of energy levels known as Zeeman splitting [26]. If the light is far-off resonance with a transition involving these levels, then the dispersion law can be approximated as

$$V(\lambda) = \frac{\alpha}{\lambda^2 - \lambda_0^2}, \quad (2)$$

where α and λ_0 are medium-dependent parameters.

Measurements of the Faraday effect and Faraday dispersion have become a staple of the undergraduate optics laboratory [27–38]. The standard technique is to use a linear polarizer after the Faraday medium to measure the rotation. The light intensity after the analyser is given by Malus' law [1],

$$I = I_0 \cos^2(\theta_A + \theta_B), \quad (3)$$

where θ_A and θ_B are the analyser angle and the additional rotation induced by the Faraday effect, respectively. Figure 1 shows the prediction of this equation as a function of θ_A and λ , where the wavelength dependence is obtained from (1) and (2).

To characterise Faraday dispersion, we can either measure the rotation at discrete wavelengths [35, 37] (vertical lines in figure 1) or at all wavelengths simultaneously using white light [22] (horizontal lines in figure 1). The white-light technique has also been used to measure optical rotation in other circularly birefringent media such as sugar solutions [39]. White-light has the advantage that only one source is required but the disadvantage that we also require a spectrometer.

In this paper, we compare measurements of the Verdet constant of terbium gallium garnet (TGG) using white-light and discrete laser wavelengths. We show that the two techniques have different strengths and weaknesses. Whereas the white-light technique can be easily implemented using a single light source, the potential for systematic errors is problematic. By contrast, the discrete-wavelength technique necessitates the use of many lasers to measure the Faraday dispersion, with a concomitant larger overhead. However, the close to ideal nature of laser sources, including a well-defined centre wavelength, small beam divergence and low intensity fluctuations makes the laser method less prone to systematic errors.

2. Experiment

The experimental set up is shown in figure 2. It consists of a light source, either (a) a fibre optic white light source or (b) a laser (Photonics Technology HEXA-BEAM which provides up to six wavelengths in a single head) with power less than 1 mW. The light is collimated and

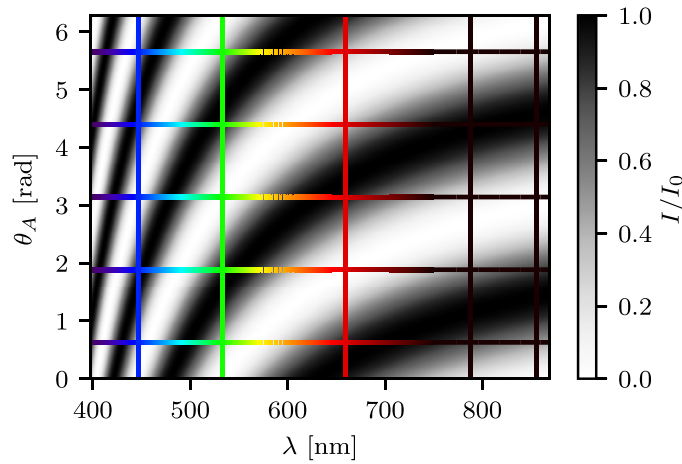


Figure 1. The normalised light intensity, I/I_0 given by (3), incident on the detector as a function of wavelength, λ , and the analyser angle, θ_A . To determine the Faraday rotation, we can either fix the wavelength and vary θ_A (vertical lines), or fix θ_A and measure at different wavelengths e.g. using white light (horizontal lines). The band-like structure is caused by the polarisation rotating in and out of alignment with the second polariser.

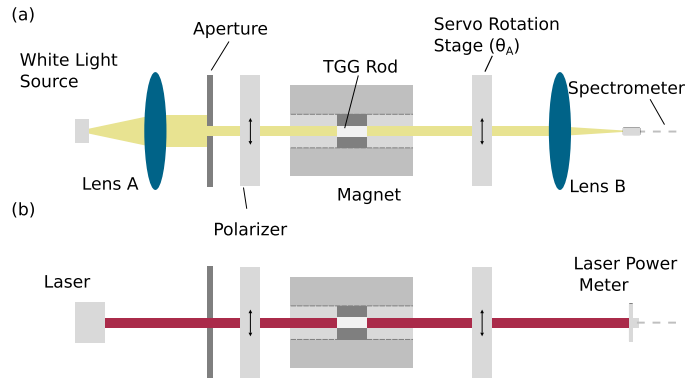


Figure 2. (a) Experimental setup for white-light methods. Lens A is used for collimation and lens B is used to focus the light beam onto an optic fibre connected to a spectrometer. (b) Experimental setup for discrete wavelength methods. In both setups, the first polariser is used to generate linearly polarised light in a known orientation and the second is used to determine the change in polarisation. Note the angle of the second polariser (θ_A) is taken with respect to the angle of the first.

passes through a linear polarizer then a TGG crystal placed inside a permanent magnet. The magnet produces an axial field with maximum field strength, $B_{\max} = 1.62 \text{ T}$ [40]. The spatial variation of the field is discussed in appendix A. After the magnet, the light passes through a second polarizer, the analyser. The analyser angle, θ_A , is controlled by a motorized rotation stage. Finally, the transmitted intensity is recorded using either (a) a spectrometer or (b) a power metre.

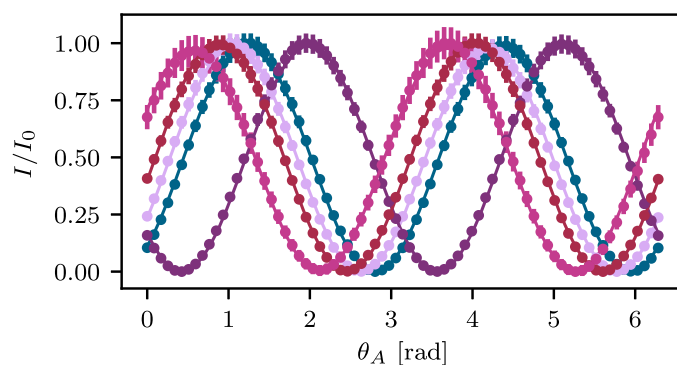


Figure 3. Plots of the normalized intensity obtained with the discrete wavelength method against analyser angle for each laser. The laser wavelengths are identified by colour as follows—blue: 446.6 nm; violet: 533.1 nm; purple: 659.2 nm; red: 787.5 nm; pink: 855.1 nm.

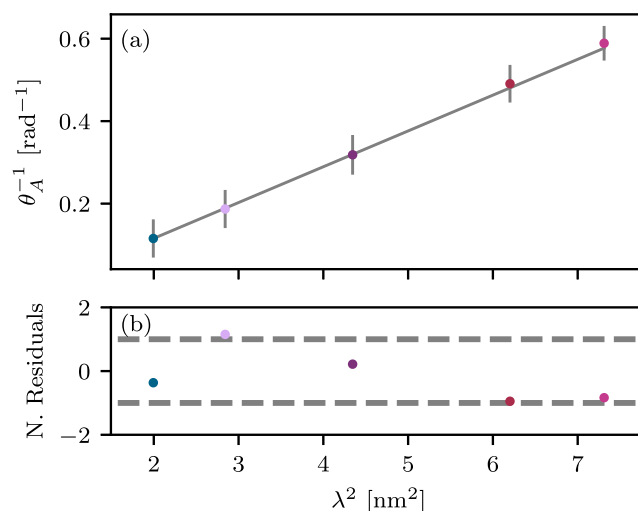


Figure 4. Discrete wavelength fit: a plot of the inverse rotation angle computed for each wavelength against λ^2 is shown in (a) with normalized residuals shown in (b). The laser wavelengths are identified by colour as follows: blue—446.6 nm; violet—533.1 nm; purple—659.2 nm; red—787.5 nm; pink—855.1 nm.

For the laser source, first the wavelength is fixed and θ_A is varied (vertical cuts in figure 1). Subsequently this is repeated for a different laser wavelength. For the white-light source, all wavelengths are measured simultaneously (horizontal cuts in figure 1). In the white-light case, θ_A can also be varied to record different horizontal cuts. Detailed accounts of the experimental methods are given in the subsequent sections.

Table 1. Values obtained from the fits to the data obtained with each laser in the discrete wavelength method. $\Delta\theta$ is the angle of rotation modulo 2π .

λ (nm)	$\Delta\theta$ (rad)	Uncertainty $\Delta\theta$ (rad)	Reduced χ^2
446.6	2.38	0.05	1.16
533.1	2.21	0.05	1.04
659.2	3.14	0.05	13.9
787.5	2.04	0.05	0.796
855.1	1.70	0.04	0.103

3. Results

The results obtained using both the white-light source and the discrete wavelength source are presented in this section. First we consider the discrete laser wavelength measurements.

3.1. Discrete laser wavelength results

The normalised intensity transmission as a function of analyser angle, θ_A , for five laser wavelengths is shown in figure 3. By comparing traces with and without the crystal, the rotation angle arising from the Faraday effect can be extracted for each wavelength. These data are plotted against λ^2 in figure 4 and manifest as a straight line as expected from (1) and (2). A straight line fit using weighted linear regression [41] allows the parameters α and λ_0 to be extracted.

The parameters obtained for each laser wavelength, λ , are given in table 1. The Verdet dispersion coefficients were found to be: $\alpha = (44.3 \pm 0.6) \times 10^{-12}$ rad mT $^{-1}$; and $\lambda_0 = (258 \pm 1)$ nm. The reduced χ^2 value in the fit was $\chi_{\text{red}}^2 = 0.41$. In order to obtain a suitable value of χ^2 , the uncertainties in the rotation angles (see table 1) were scaled by a factor n found by gradient descent with a cost function of the form $(\chi_{\text{red}}^2 - 1)^2$.

3.2. White-light results

The data obtained using the white-light method are depicted in figure 5. First, the spectrum with and without the second polarizer is shown in figure 5(a). Even before we add the analyzer, the transmitted spectrum is relatively complex consisting of the spectrum of the source modified by absorption in the crystal. For TGG, there is a strong absorption at around 480 nm, marked by a pronounced dip in the transmitted intensity. The addition of the analyzer yields broad minima at wavelengths where the Faraday effect rotates the plane of polarization to be orthogonal to the transmission axis of the analyzer. In figure 5(a) this occurs at around 450 nm and 550 nm. In principle, this spectrum provides all the information we need to extract the Faraday dispersion curve. However, due to the variation of the background intensity, how best to extract the results from the data is not obvious. We shall explore two methods. First, we fit to the whole spectrum in figure 5. We call this the complete spectrum method. Second, we fit only to the maxima and minima. We call this the stationary point method.

3.2.1. White-light complete spectrum method. In this first method, the complete spectrum is fitted. We assume that the normalised transmission is given by the product of the normalised spectrum of the source and Malus' law with the wavelength dependent Faraday rotation angle given by (1) and (2). This was repeated for spectra taken with a selection of analyser angles, the results of which are shown in figure 6. From these fits, the dispersion law can be extracted in a similar way to that described in [39].

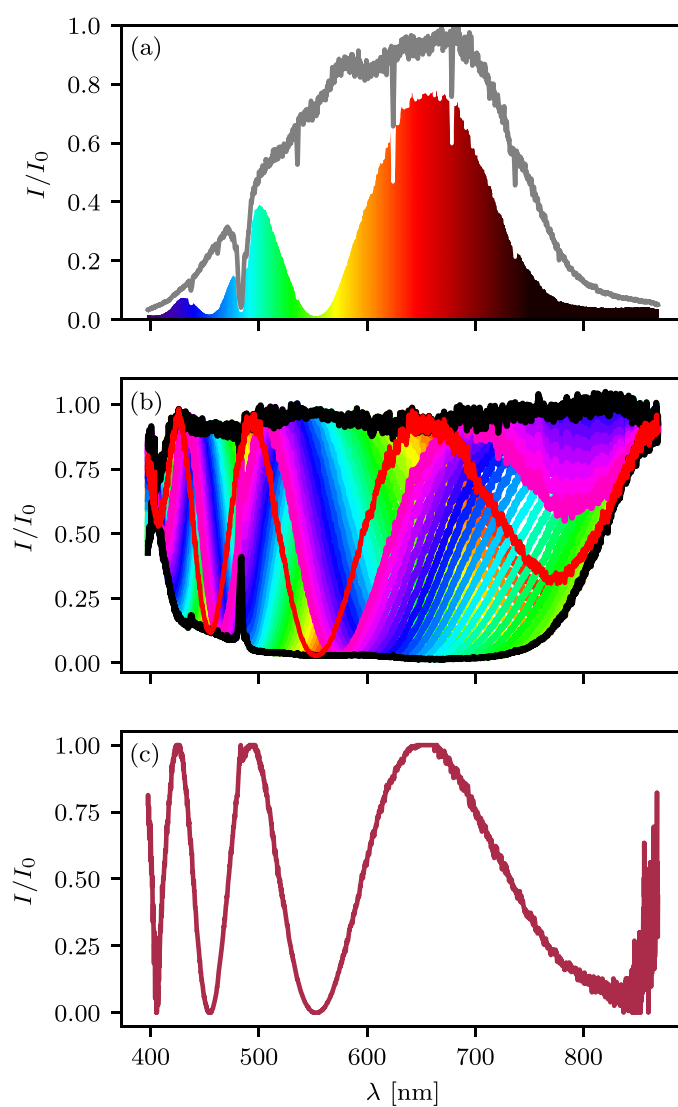


Figure 5. The normalised transmission spectrum for the white light source through the crystal is shown in grey in plot (a); $I_0 = 0.8 \mu\text{W cm}^{-2} \text{nm}^{-1}$. Adding linear polarizers aligned parallel on either side of the crystal produces the spectrum shown in colour in plot (a). Partially normalised transmittance spectra for analyser angles ($\theta \in [0^\circ, 90^\circ]$) are shown in colour in plot (b) with the corresponding maximum and minimum values at each wavelength shown in black. The coloured spectra in (b) were re-normalised to lie between the black lines prior to further processing—the re-normalised spectrum for an analyser angle of 0° is shown in plot (c). The poor signal to noise seen for wavelengths greater than approximately 800 nm is a consequence of the low light level in this part of the spectrum.

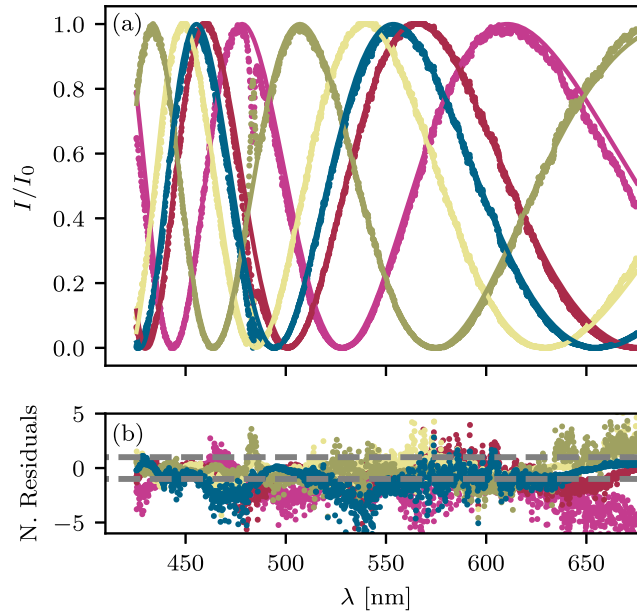


Figure 6. Single spectrum polarimetry: the normalized data and associated fits for analyser angles -3.717 , -1.327 , -1.858 , -5.841 and -4.690 are shown in pink, red, yellow, green and blue respectively for the wavelengths 425 nm–675 nm in (a). The normalised residuals are shown in (b).

Table 2. Dispersion characterisation obtained using the complete spectrum polarimetry method for five randomly selected analyser angles. The reduced χ^2 values and Durbin Watson (\mathcal{D}) statistics for each data set are also given.

θ_A (rad)	α (10^{-12} rad mT $^{-1}$)	λ_0 (nm)	χ_{red}^2	\mathcal{D}
-3.717	44.6(6)	241.39(2)	7.168	0.212
-1.327	44.5(6)	242.40(2)	1.558	0.229
-1.858	44.3(6)	242.32(2)	1.039	0.354
-5.841	44.0(6)	244.17(2)	1.482	0.248
-4.690	44.2(6)	243.78(2)	2.927	0.207

The results obtained with complete spectrum polarimetry are given in table 2. The associated normalised data and fits are shown in figure 6. The mean parameter values obtained are $\alpha = (44.3 \pm 0.2) \times 10^{-12}$ rad mT $^{-1}$, $\lambda_0 = (243.2 \pm 0.7)$ nm. Note that the relatively low Durbin Watson \mathcal{D} statistics given in table 2 suggest a positive correlation in the residuals.

3.2.2. White-light stationary point method. In this second method, only the intensity minima and maxima are fitted. The wavelengths corresponding to these stationary points were found for a range of analyzer angles using the method illustrated in figure 7(a).

Accurate values for the stationary points can be found by fitting a quadratic function around each maximum and minimum (see figure 7(a)). These stationary points are associated with particular rotation angles; specifically, for maxima ($\theta_B + \theta_A = n\pi$), and, for minima ($\theta_B + \theta_A = (n + 1/2)\pi$) with $n \in \mathbb{Z}$. Changing the analyser (θ_A) changes the wavelength at which the

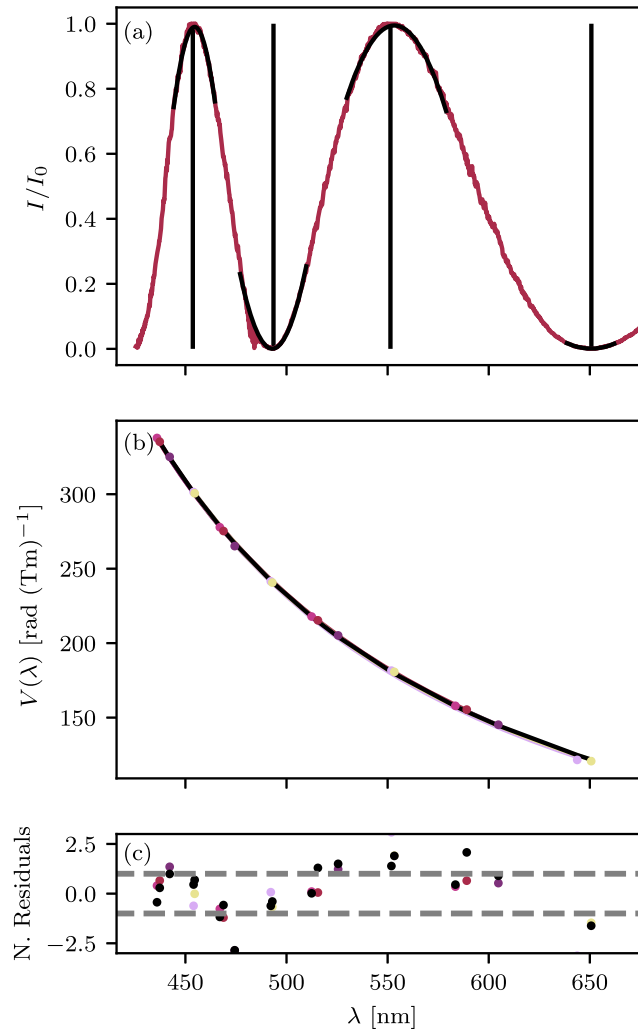


Figure 7. Stationary point identification: quadratic functions (shown in black in (a)) were fitted to the stationary points of the normalised spectra (where $I_0 = 0.5 \mu\text{W cm}^{-2} \text{nm}^{-1}$) to determine their location. This process was repeated for five different analyser angles and the Faraday rotation and hence Verdet constant associated with each stationary point was calculated; these data are shown in (b). Individual fits to each of the five data sets were found along with a fit using all of the data. The normalised residuals from these fits are shown in (c) with the residuals from the fit using all the data shown in black. Approximately two thirds of the normalised residuals lie within the interval ± 1 , as is expected for a good fit [41].

stationary points occur. From (1) and (3) these values of rotation angles are used to determine the Verdet constant for discrete wavelengths, giving the curve shown in figure 7(b).

The results obtained with the stationary point values extracted from figure 7 are summarised in table 3. The parameters obtained by combining results for 72 different analyser angles, see figure 8, are $\alpha = (44.6 \pm 0.6) \times 10^{-12} \text{ rad mT}^{-1}$, $\lambda_0 = (241.0 \pm 0.2) \text{ nm}$. The reduced χ_{red}^2 for this sample was 1.367.

Table 3. Dispersion characterisation values obtained by fitting stationary points at five randomly selected analyser angles. Using all five data sets $\alpha = 44.4(6) \times 10^{-12} \text{ rad mT}^{-1}$ and $\lambda_0 = 242.1(7) \text{ nm}$ and the reduced χ^2 value was found to be 3.059.

θ_A (rad)	α ($10^{-12} \text{ rad mT}^{-1}$)	λ_0 (nm)	χ_{red}^2
-3.717	44.5(6)	241(2)	0.444
-2.212	45.0(6)	239(2)	1.155
-2.478	44.6(6)	241(2)	5.910
-3.097	43.6(6)	248.4(9)	9.836
-4.690	44.3(6)	243(2)	3.131

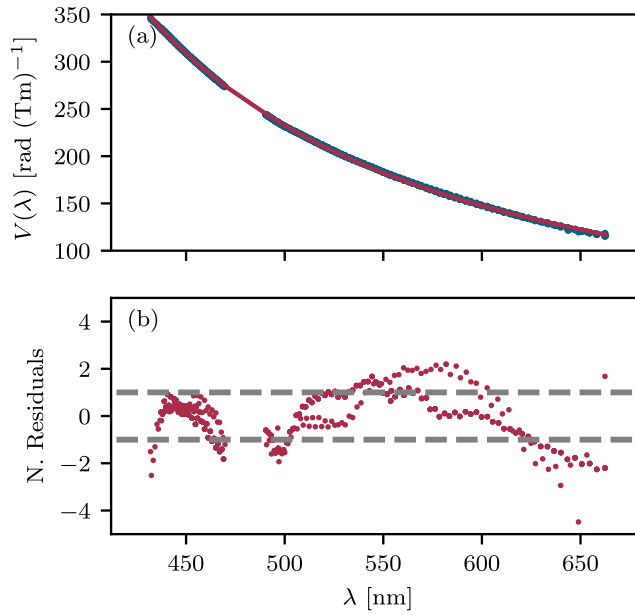


Figure 8. Stationary points for 72 different analyser angles (depicted in blue in (a)) along with a fit through these data (shown in red). The resulting normalised residuals are shown in (b).

4. Comparison of the different methods

We have introduced two experimental methods to measure the Faraday dispersion law, white-light versus discrete laser wavelength, and two ways to analyse the white-light spectra (fitting only the maxima and minima or fitting the whole spectrum). As there are only two parameters, the results of all three methods are summarised using error surfaces, see figure 9. Note that the laser and white-light measurements disagree systematically, with the laser measurement returning a value closer to the literature values [42]. There are at least two possible ways to explain the systematic error in the white light measurements. First, the lasers and white-light sample different regions in the crystal. This could lead to systematic errors in the white-light measurement due to spatial inhomogeneities. Additionally, as the white light source is less well-collimated it is more difficult to align the light through the centre. Second, the white-light is partially absorbed by the crystal, as is evident from the prominent absorption features in

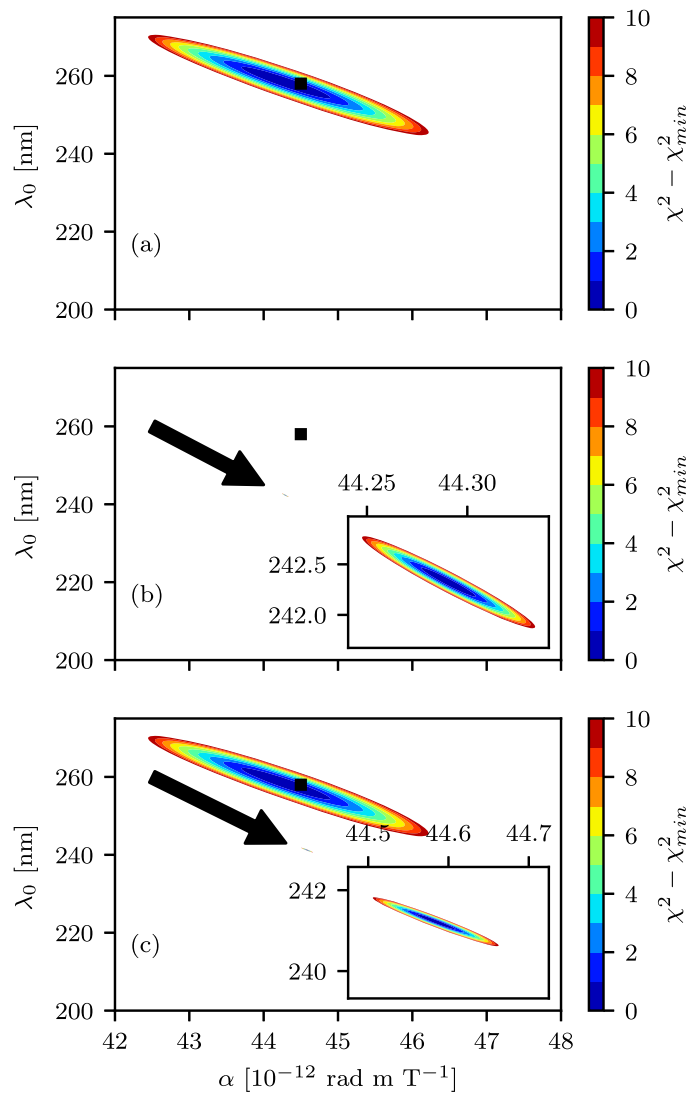


Figure 9. Contour plots depicting the reduced χ^2 value as a function of α and λ_0 for the three methods. The results for the discrete wavelength method are shown in (a). The results for the single spectrum polarimetry method are shown in (b) for an analyser angle of -1.858 rad. The results for the stationary point method are marked with an arrow in (c) with (a) depicted above for reference. The black squares in each of the plots indicate the literature values for α and λ_0 [42].

figure 5. This causes heating potentially leading to a systematic error as the Verdet constant of TGG is highly temperature dependent [21, 26].

5. Conclusion

In this paper we compare discrete versus continuous frequency measurements to characterise Faraday dispersion in an optical medium. The discrete method uses multiple lasers with different wavelengths. The continuous (or white-light) method uses a single broadband source to measure over a wide range of wavelengths simultaneously. Although the discrete method carries the overhead of requiring many sources it is simpler to implement and for the case of TGG crystal studied is less prone to systematic errors.

Acknowledgments

The authors thank Jacque Vigué for supplying the magnet, Francisco Ponciano Ojeda for assistance with the magnet and designing the rod holder, and Durham University for providing the equipment. We thank Jason Anderson and Aidan Hindmarch for development of the experimental apparatus.

Appendix A. Field characterisation

An accurate knowledge of the field strength within the TGG crystal is required to determine the Verdet dispersion. To characterise this field, a Hall probe was used to measure its strength, periodically, along one axial and one transverse path through the centre of the magnet. These data were then extrapolated to find the 3D distribution of field strength (see figure A1). From this, the length integral of \mathcal{B} was determined. The axial field integral ($\int_0^\ell \mathcal{B}(0, 0, z) dz$) was found to have a value of 25.3 T mm, whereas the average over the crystal cross-sectional area, A , was found to be $(1/A) \int_0^\ell \mathcal{B}(x, y, z) dx dy dz = 26.2 \pm 0.3$ T mm.

A.1. Uncertainty in $\int \mathcal{B} dl$

The uncertainty in $\int \mathcal{B} dl$ was determined by calculating the integral along an axial path through the magnet and calculating the integral for the same path translated axially (by the uncertainty in axial position) and taking the difference. The uncertainty in the axial position of the crystal was taken to be ± 3 mm. The corresponding uncertainty in the average integral $(1/A) \int_0^\ell \mathcal{B}(x, y, z) dx dy dz$ was found to be ± 0.3 T mm.

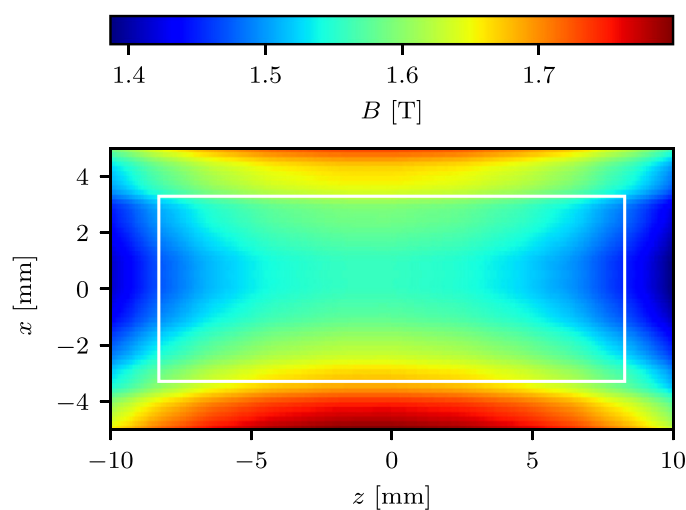


Figure A1. The magnetic field strength around the centre of the bore hole as a function of transverse (x) and axial (z) position found by extrapolating measurements in transverse and axial directions intersecting the centre. The location of the crystal is outlined by a white rectangle.

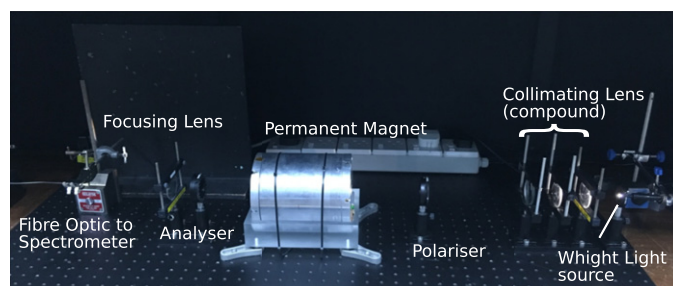


Figure B1. Photograph of the experimental setup for the white light methods. Note that the servo rotation stage has been omitted from the analyser in this image. Additionally, a compound lens was used to produce a more tightly collimated beam.

Appendix B. Specific experimental setup

Specific details of the experimental apparatus used in this work are provided here to aid with reproducibility. An image of the apparatus used in the white light method is shown in figure B1.

The white light source used in this investigation was Schott KL 1500 HAL, the spectrum of which is shown in figure B2.

The permanent magnet used in this work was constructed from a series of ring segments with both radial and axial polarities. The central bore, in which the TGG sample was placed, had a radius of 11 mm. Precise details of the magnet's construction are given in [40] under the section pertaining to prototype 3. The spectrometer used was an IS Instruments Miniature Spectrometer and a Thor Labs S120C Si Photodiode was used as the LASER power metre.

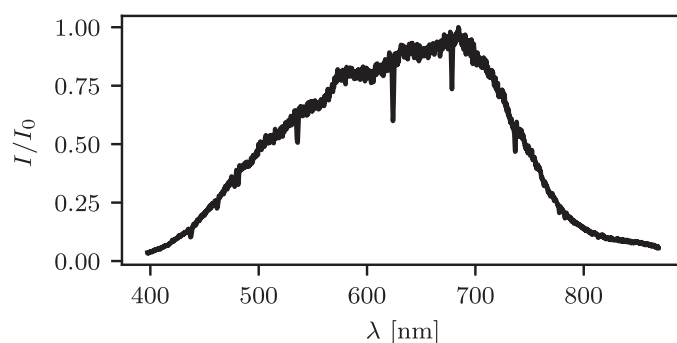


Figure B2. Normalised intensity spectrum (where $I_0 = 0.8 \mu\text{W cm}^{-2} \text{ nm}^{-1}$) of Schott KL 1500 HAL—measured with the TGG crystal and polariser absent from the setup depicted in figure B1.

ORCID iDs

James L Maxwell  <https://orcid.org/0000-0002-3125-9280>

Ifan G Hughes  <https://orcid.org/0000-0001-6322-6435>

References

- [1] Adams C S and Hughes I G 2018 *Optics F2f: From Fourier to Fresnel* (Oxford: Oxford University Press)
- [2] Sansalone F J 1971 Compact optical isolator *Appl. Opt.* **10** 2329–31
- [3] Adams C S and Ferguson A I 1990 Saturated spectroscopy and two-photon absorption spectroscopy in rubidium using an actively stabilised Ti:Al₂O₃ ring laser *Opt. Commun.* **75** 419–24
- [4] Weller L, Kleinbach K S, Zentile M A, Knappe S, Hughes I G and Adams C S 2012 Optical isolator using an atomic vapor in the hyperfine Paschen–Back regime *Opt. Lett.* **37** 3405–7
- [5] Yeh P 1982 Dispersive magneto-optic filters *Appl. Opt.* **21** 2069–75
- [6] Dick D J and Shay T M 1991 Ultrahigh-noise rejection optical filter *Opt. Lett.* **16** 867–9
- [7] Abel R P, Krohn U, Siddons P, Hughes I G and Adams C S 2009 Faraday dichroic beam splitter for Raman light using an isotopically pure alkali-metal-vapor cell *Opt. Lett.* **34** 3071–3
- [8] Zielińska J A, Beduini F A, Lucivero V G and Mitchell M W 2014 Atomic filtering for hybrid continuous-variable/discrete-variable quantum optics *Opt. Express* **22** 25307–17
- [9] Kiefer W, Löw R, Wrachtrup J and Gerhardt I 2014 Na-Faraday rotation filtering: the optimal point *Sci. Rep.* **4** 6552
- [10] Zentile M A, Keaveney J, Mathew R S, Whiting D J, Adams C S and Hughes I G 2015 Optimization of atomic Faraday filters in the presence of homogeneous line broadening *J. Phys. B: At. Mol. Opt. Phys.* **48** 185001
- [11] Zentile M A, Whiting D J, Keaveney J, Adams C S and Hughes I G 2015 Atomic Faraday filter with equivalent noise bandwidth less than 1 GHz *Opt. Lett.* **40** 2000–3
- [12] Gerhardt I 2018 How anomalous is my Faraday filter? *Opt. Lett.* **43** 5295–8
- [13] Keaveney J, Wrathmall S A, Adams C S and Hughes I G 2018 Optimized ultra-narrow atomic bandpass filters via magneto-optic rotation in an unconstrained geometry *Opt. Lett.* **43** 4272–5
- [14] Higgins C R, Pizzey D, Mathew R S and Hughes I G 2020 Atomic line versus lens cavity filters: a comparison of their merits *OSA Continuum* **3** 961–70
- [15] Cimino M, Cacciani A and Soprani N 1968 An instrument to measure solar magnetic fields by an atomic-beam method *Sol. Phys.* **3** 618–22
- [16] Cacciani A, Ricci D, Rosati P, Rhodes E J, Smith E, Tomczyk S and Ulrich R K 1990 Solar magnetic fields measurements with a magneto-optical filter *Il Nuovo Cimento C* **13** 125–30

- [17] Xia Y, Cheng X, Li F, Yang Y, Lin X, Jiao J, Du L, Wang J and Yang G 2020 Sodium lidar observation over full diurnal cycles in Beijing, China *Appl. Opt.* **59** 1529
- [18] Popescu A, Schorstein K and Walther T 2004 A novel approach to a LIDAR for remote sensing of the ocean temperature *Appl. Phys. B* **79** 955–61
- [19] Huang W *et al* 2009 Field demonstration of simultaneous wind and temperature measurements from 5 to 50 km with a Na double-edge magneto-optic filter in a multi-frequency Doppler lidar *Opt. Lett.* **34** 1552–4
- [20] Kudenov M W, Pantalone B and Yang R 2020 Dual-beam potassium Voigt filter for atomic line imaging *Appl. Opt.* **59** 5282–9
- [21] Barnes N P and Petway L B 1992 Variation of the Verdet constant with temperature of terbium gallium garnet *J. Opt. Soc. Am. B* **9** 1912–5
- [22] Vasylyev V, Villora E G, Nakamura M, Sugahara Y and Shimamura K 2012 UV-visible Faraday rotators based on rare-earth fluoride single crystals: LiREF_4 ($RE = \text{Tb, Dy, Ho, Er}$ and Yb), PrF_3 and CeF_3 *Opt. Express* **20** 14460–70
- [23] Hasegawa Y *et al* 2008 Remarkable magneto-optical properties of europium selenide nanoparticles with wide energy gaps *J. Am. Chem. Soc.* **130** 5710–5
- [24] Louant O, Liégeois V, Verbiest T, Persoons A and Champagne B 2017 Faraday effect in stacks of aromatic molecules *J. Phys. Chem. C* **121** 15348–52
- [25] Nelson Z, Delage-Laurin L, Peeks M D and Swager T M 2021 Large Faraday rotation in optical-quality phthalocyanine and porphyrin thin films *J. Am. Chem. Soc.* **143** 7096–103
- [26] Slezák O, Yasuhara R, Lucianetti A and Mocek T 2016 Temperature-wavelength dependence of terbium gallium garnet ceramics Verdet constant *Opt. Mater. Express* **6** 3683–91
- [27] Loeffler F J 1983 A Faraday rotation experiment for the undergraduate physics laboratory *Am. J. Phys.* **51** 661–3
- [28] Pedrotti F L and Bandettini P 1990 Faraday rotation in the undergraduate advanced laboratory *Am. J. Phys.* **58** 542–5
- [29] Briggs E M and Peterson R W 1993 Liquid cell Faraday modulator *Am. J. Phys.* **61** 186–7
- [30] Van Baak D A 1996 Resonant Faraday rotation as a probe of atomic dispersion *Am. J. Phys.* **64** 724–35
- [31] Jain A, Kumar J, Zhou F, Li L and Tripathy S 1999 A simple experiment for determining Verdet constants using alternating current magnetic fields *Am. J. Phys.* **67** 714–7
- [32] Valev V K, Wouters J and Verbiest T 2008 Differential detection for measurements of Faraday rotation by means of ac magnetic fields *Eur. J. Phys.* **29** 1099–104
- [33] Valev V K, Wouters J and Verbiest T 2008 Precise measurements of Faraday rotation using ac magnetic fields *Am. J. Phys.* **76** 626–9
- [34] Patterson L H C, Kihlstrom K E and Everest M A 2015 Balanced polarimeter: a cost-effective approach for measuring the polarization of light *Am. J. Phys.* **83** 91–4
- [35] Compton R N and Duncan M A 2016 *Laser Experiments for Chemistry and Physics* (Oxford: Oxford University Press)
- [36] Hunte C 2018 A modulation technique for the measurement of the DC longitudinal Faraday effect *Eur. J. Phys.* **39** 025301
- [37] Carr D L, Spong N L R, Hughes I G and Adams C S 2020 Measuring the Faraday effect in olive oil using permanent magnets and Malus' law *Eur. J. Phys.* **41** 025301
- [38] Al-Basheer W 2020 Verdet constant determination of dielectric media using a new versatile, portable and low-cost magneto-optical rotator *Eur. J. Phys.* **41** 045804
- [39] Anderson J, Gillen C, Wright J, Adams C S and Hughes I G 2020 Optical rotation of white light *Am. J. Phys.* **88** 247–51
- [40] Tréneç G, Volondat W, Cugat O and Vigué J 2011 Permanent magnets for Faraday rotators inspired by the design of the magic sphere *Appl. Opt.* **50** 4788–97
- [41] Hughes I G and Hase T P A 2010 *Measurements and Their Uncertainties* (Oxford: Oxford University Press)
- [42] Molina P, Vasylyev V, Villora E and Shimamura K 2011 CeF_3 and PrF_3 as UV-visible Faraday rotators *Opt. Express* **19** 11786–91